Wigner representation of ionization and scattering in strong laser fields

C. Baumann and H.-J. Kull*
Institute for Theory of Statistical Physics, RWTH Aachen University, 52056 Aachen, Germany

G. M. Fraiman†
Institute of Applied Physics, Russian Academy of Sciences, Nizhny Novgorod, Russia
(Received 1 September 2015; published 23 December 2015)

The interaction of single-electron atoms with a strong laser field is studied in the Wigner representation. The Wigner function is a quasiprobability function in phase space that allows one to study position-momentum correlations. These correlations give a physical interpretation of the emergence of the above-threshold-ionization (ATI) energy spectrum. Conversely, the quantum-mechanical interference between electrons from neighboring photon orders can explain the spatial bunching of the electron density by the laser field. Furthermore, the Wigner function offers one a rather accurate and relatively efficient quasiclassical estimate of the bound-state population. This method is applied to laser-induced electron-ion scattering and the stationary regime of the bound-state population can be determined. The present calculations are performed for a one-dimensional Rosen-Morse potential. Extensions to general spherically symmetric atomic potentials are indicated.

DOI: 10.1103/PhysRevA.92.063420 PACS number(s): 32.80.Fb, 32.80.Rm, 52.38.Dx

I. INTRODUCTION

The behavior of atoms in strong laser fields is of fundamental importance for present-day laser physics and technology [1]. The ionization of atoms in strong fields is known as above-threshold ionization (ATI) [2], leading to electron energies of very high multiphoton orders. Recombination in strong laser fields can be applied to the generation of high-order harmonics [3] and to the production of attosecond pulses. Scattering and rescattering are likewise important multiphoton processes that have been studied extensively in atomic physics with important applications for inverse-bremsstrahlung absorption of laser light in plasmas [4–9]. Since most of these processes require nonperturbative methods, a number of theoretical approaches have been successfully developed in this field. These include, e.g., the strong-field approximation (SFA) [10], the related quantum-orbit approximation [11], and various computational methods for the solution of the time-dependent Schrödinger equation (TDSE) [12–14].

In this work, strong-field laser-atom interactions are studied in the Wigner representation [15]. For simplicity, the calculations are based on numerical solutions of the one-dimensional (1D) TDSE with the atom represented by a symmetric Rosen-Morse potential [16]. Generalizations to spherically symmetric atomic potentials are discussed to some extent in the final section of this paper. In the context of strong-field laser-atom interactions, the Wigner representation has apparently been studied only occasionally to visualize, e.g., stabilization [17], tunneling [18], ionization [19,20], and double ionization [21]. In a previous work, the emergence of the ATI spectrum from the Wigner phase-space distribution has been discussed but limited to laser-induced electron-ion scattering with impact velocities larger than the quiver velocity [22].

The Wigner function is a well-known quasiprobability distribution function in phase space. In contrast to a classical probability function, the Wigner function can assume both positive and negative values. Negative values indicate nonclassical behavior associated, e.g., with the interference between two plane waves. From the Wigner function one can obtain integrated probability distributions for position or momentum only. These are always positive-definite and agree with their usual quantum-mechanical definitions. The time evolution of the Wigner function is governed by a kinetic equation known as the Moyal equation [23]. Its classical counterpart is the Liouville equation.

We first analyze the ATI energy spectrum for the Rosen-Morse potential as a function of the electric field of the laser. The various multiphoton orders, their modulation, and the closing of the channels with increasing field strengths will be illustrated in a unified manner. Then the emergence of the ATI spectrum from the Wigner function is analyzed and thereby previous work on laser-induced scattering [22] is extended to laser-induced ionization with electron energies smaller than the quiver velocity. In the scattering problem, the electrons scattered in different periods of the laser field have been found separable into different wave packets. It was then possible to distinguish between interperiodic and intraperiodic interferences in the Wigner function. The corresponding interference fringes are found related to the common ATI peaks and their envelope modulations, respectively, in the energy spectrum. More definitely, the positions of the wave packets emitted in subsequent laser periods with momentum $\bar{p}$ will be spatially separated by $\Delta x = (\bar{p}\,T)/m = (2\pi\,\bar{p})/(\omega m)$ where T denotes the laser period, ω the circular frequency, and m the electron mass. The interference between localized wave packets leads to oscillations of the Wigner function in the momentum direction with the wavelength $\Delta p = (2\pi\hbar)/\Delta x = (\hbar\omega m)/\bar{p}$. Setting $\Delta p = p_{n+1} - p_n$ and $\bar{p} = (p_{n+1} + p_n)/2$, where n refers to the photon order, one obtains for the separation between subsequent energy peaks

$$\Delta E = \frac{1}{2m}p_{n+1}^2 - \frac{1}{2m}p_n^2 = \frac{1}{2m}(p_{n+1}+p_n)(p_{n+1}-p_n) = \bar{p}\,\frac{\Delta p}{m} = \hbar\omega. \quad (1)$$

*kull@ilt-extern.fraunhofer.de
†fraiman@appl.sci-nnov.ru

Interperiodic interference therefore accounts for the familiar ATI peak sequence separated by the photon energy.

In the present ionization problem, we observe a more advanced stage of the evolution, which is characterized by a coalescence of the wave packets from different periods. Coalescence occurs early since the characteristic drift momenta are smaller than the quiver momentum. It is then no longer possible to distinguish between the electrons emitted in different laser periods. However, one still obtains the ATI spectrum and can reverse the above argument. The interference between the delocalized plane waves of neighboring photon orders leads to a spatial bunching of the electron density at the average momentum $\bar{p}$ with the bunch length $\Delta x = (\bar{p}\,T)/m$. In the present work, we actually observe this spatial bunching effect. Since spatial bunching occurs at certain energies $\bar{E} = \bar{p}^2/(2m)$ only, the Wigner representation is essential to resolve its presence unambiguously. Experimental evidence of this bunching effect would be a nice confirmation of the Wigner quasiprobability in a nonclassical phase-space area.

As a second important application of the Wigner representation in laser-atom interactions, we consider the bound-state population of the atom. It will be shown, that one can obtain an accurate and efficient estimate of the bound-state population at each zero of the laser field. This estimate is defined by the quantum-mechanical probability that the electron can be found in the phase-space area enclosed by the classical separatix between bound and free orbits. Near the separatrix, the states are highly excited and the quasiclassical approximation appears therefore quite reasonable. Validations of this method in comparison with exact results show only minor differences of at most a few percent in the cases considered. We first validate this method for a Rosen-Morse potential with one bound state. Then we demonstrate its applicability for laser-induced electron-ion scattering and obtain the steady-state bound-state population in the presence of the laser field. Finally extensions of the method to spherically symmetric atomic potentials are discussed and validated for a hydrogen atom. It is noted that the calculation of bound-state populations from the wave function in configuration space is often a cumbersome procedure. According to the quantum-mechanical definition, the populations of the bound states are obtained by projections on the energy eigenstates of the atomic Hamiltonian. Exact calculations, requiring the knowledge of a complete set of energy eigenstates, are rarely feasible. To avoid such extensive atomic physics calculations one often uses other approximations, e.g., the spatial volume method [24–26], the spatial surface-flux method [27], the resolvent-operator technique [28], or the window-operator method [29,30]. The present approach is based on the quantum-mechanical quasiprobability given by the Wigner function and the quasiclassical behavior near the ionization threshold in phase space. It has the advantage that it can be applied instantaneously, since a spatial separation of free and bound parts of the wave function is not required.

This paper is organized as follows: In Sec. II, the physical model, including the atomic potential and the laser field, is introduced. Atomic units will be used if not otherwise stated. In Sec. III, ionization of the model atom by the laser field is considered. Energy spectra and Wigner functions are calculated to discuss the dynamic Stark shift, channel closing, as well as coalescence and bunching in phase space. In Sec. IV, the quasiclassical method for calculating the bound-state population by the Wigner function is presented. Validations of this method, applications to laser-driven electron-ion scattering, and extensions to spherically symmetric potentials are discussed.

II. BASIC EQUATIONS

The time evolution of the wave function $\psi(x,t)$ is subjected to the TDSE and reads in atomic units ($\hbar = m_e = e = 1$)

$$i\,\partial_t \psi(x,t) = H\psi(x,t),$$
$$H = -\tfrac{1}{2}\partial_x^2 + V(x) + x\mathcal{E}(t), \tag{2}$$

where $V(x)$ stands for an atomic potential and $\mathcal{E}(t)$ represents the electromagnetic light wave in the electric-dipole approximation.

Due to the linear coupling of electric field and position in (2), a small time step is required to propagate the wave function numerically in time. It is therefore convenient to describe the interaction with the laser field in the so-called Kramers-Henneberger (KH) frame [31,32]. It is an accelerated reference frame attached to the quiver motion of the electron. Performing the transformations

$$\widetilde{\psi}(x,t) = \exp\left(-ix\dot{\xi}(t) + \frac{i}{2}\int_0^t dt'\,\dot{\xi}^2(t')\right)\psi(x,t) \tag{3}$$

and

$$\phi(u,t) = \widetilde{\psi}(u+\xi(t),t), \tag{4}$$

where $\xi(t)$ obeys the classical equation of motion of the electron in the electric field, $\ddot{\xi}(t) = -\mathcal{E}(t)$, the TDSE for the wave function $\phi(u,t)$ in the KH frame becomes

$$i\,\partial_t \phi(u,t) = \left\{-\tfrac{1}{2}\partial_u^2 + V(u+\xi(t))\right\}\phi(u,t). \tag{5}$$

The interaction with the light wave is now contained in the time-dependent displacement of the atomic potential. In the present work, the Rosen-Morse potential [16]

$$V(x) = -\frac{1}{\cosh^2(x)} \tag{6}$$

is used in all 1D calculations. In the absence of a laser field, this model potential is reflectionless and it has only one bound eigenstate,

$$\psi_0(x,t) = \frac{1}{\sqrt{2}\cosh(x)}e^{-iE_0 t}, \tag{7}$$

where $E_0 = -0.5$ stands for its energy [33].

The electric field is approximated by a monochromatic sine wave,

$$\mathcal{E}(t) = \mathcal{E}_0 \sin(\omega t), \tag{8}$$

with field strength $\mathcal{E}_0$ and frequency ω. For a given initial wave function $\phi(u,t=0) = \phi_0(u)$, the TDSE (5) has been solved numerically by using a fast-Fourier-transform (FFT) split-operator method [34]. In the simulations, step sizes of $\Delta x = 0.1$ and $\Delta t \approx 0.01$ have been used, which turned out to be adequate.

The Wigner function enables a description of a quantum-mechanical state in a phase space. It can be calculated from

the position representation of the wave function [15],

$$W(p,q) = \int_{-\infty}^{\infty} dr\, \psi\left(q + \frac{r}{2}\right)\psi^*\left(q - \frac{r}{2}\right)e^{-ipr}. \quad (9)$$

According to its definition, the Wigner function is real valued. However, it can take on positive as well as negative values in contrast to classical phase-space probability density functions. Because of this property, the Wigner function allows one for the identification of quantum-mechanical behavior.

III. LASER-INDUCED IONIZATION

To be able to study the laser-induced ionization of the model atom (6), the system has to be prepared in its ground state at the initial time $t = 0$. Resulting from (3), (4), and (7), the initial wave function in the KH frame has to be chosen as

$$\phi_0(x) = \frac{1}{\sqrt{2}\cosh(x)} \exp(i\dot{\xi}_0 x). \quad (10)$$

Here $\dot{\xi}_0 = \mathcal{E}_0/\omega$ symbolizes the underlying quiver momentum at the initial time.

In the simulations, frequencies of $\omega = 0.1$ and $\omega = 0.2$ ($\omega = 0.2$ corresponds to a wavelength of 225 nm and to a photon energy of $\hbar\omega = 5.5$ eV) and field strengths $\mathcal{E}_0$ between 0.06 and 0.28 (associated with intensities of 0.13–2.75 PW/cm^2) have been used to parametrize the laser. Such parameters can be achieved by present-day free-electron lasers [35] and frequency-upconverted short-pulse lasers [36].

A. Energy distribution outside the laser field

Energy spectra of the unbound electrons are subsequently discussed. In the KH frame, the spectrum characterizes the probability density of detecting an electron with drift energy $E = k^2/2$ outside the laser field and has been defined by

$$f(E) = \frac{1}{2\pi|k|}\{|\hat{\phi}_{\text{free}}(k)|^2 + |\hat{\phi}_{\text{free}}(-k)|^2\}, \quad (11)$$

with the states $\hat{\phi}_{\text{free}}(k)$ that are representing the freed electron in the k space. They have been calculated from the position representation of the free-electron states by using spatial Fourier transforms. Based on the single bound state of the model atom, the determination of the free states $\phi_{\text{free}}(x,t)$ can be performed in the standard manner by subtracting the projection on the ground state,

$$\begin{aligned}\phi_{\text{free}}(x,t) &= \phi(x,t) - \rho(t)\,\phi_0(x,t),\\ \rho(t) &= \int_{-\infty}^{\infty} dy\, \phi_0^*(y,t)\phi(y,t).\end{aligned} \quad (12)$$

At this point one has to keep in mind the time dependence of $\phi_0(x,t)$ in the KH frame.

By energy conservation, one expects drift energies at

$$E = n\omega - |E_0| - \frac{\mathcal{E}_0^2}{4\omega^2}, \quad (13)$$

where n stands for the number of absorbed photons and $\mathcal{E}_0^2/(4\omega^2)$ accounts for the dynamic Stark shift of the continuum states by the ponderomotive potential. Figure 1 finally shows the variation of the energy distribution with the field strength $\mathcal{E}_0$ for a laser with frequency $\omega = 0.1$ after the interaction time of $3T$ ($T = 2\pi/\omega$ is the laser period). One can clearly recognize the formation of discrete stripes, indicating the quadratic dependence of the drift energy on the field strength due to (13). Neighboring stripes are shifted in the E direction by the photon energy ω, which characterizes the ATI spectrum. Consequently, each stripe is associated with the corresponding number of absorbed photons n. However, instead of displaying a continuous profile the discrete stripes consist of islandlike areas of high spectral densities. This insular behavior yields a modulation of the spectrum which has been previously observed in the case of scattering spectra, where the modulations could be ascribed to the intraperiodic quantum interference of electron trajectories [22]. Beyond, Fig. 2 illustrates energy spectra for different laser-field strengths in a field with frequency $\omega = 0.2$. It can be seen that an increase of the intensity reduces the drift energy of the outgoing electron. Considering especially the threshold strength $\mathcal{E}_0 = 0.13$, the lowest ATI peak vanishes due to the fact that three-photon absorption is insufficient to transfer a finite drift energy to the electron. The closing of an ionization channel is subsequently discussed in the framework of the Wigner function.

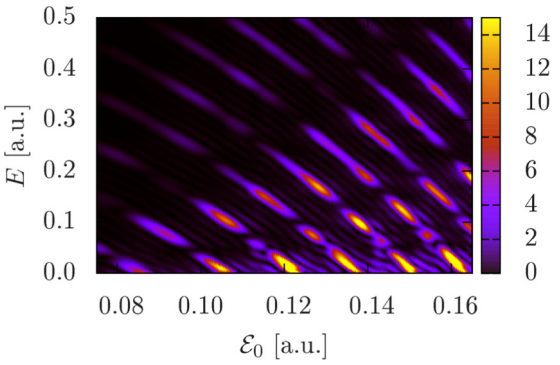

FIG. 1. (Color online) Spectral density as a function of electric field strength $\mathcal{E}_0$ and drift energy E, recorded for a laser with frequency $\omega = 0.1$ after an interaction time of three laser periods. According to (13), the absorption of $n = 7, \ldots, 16$ photons is shown.

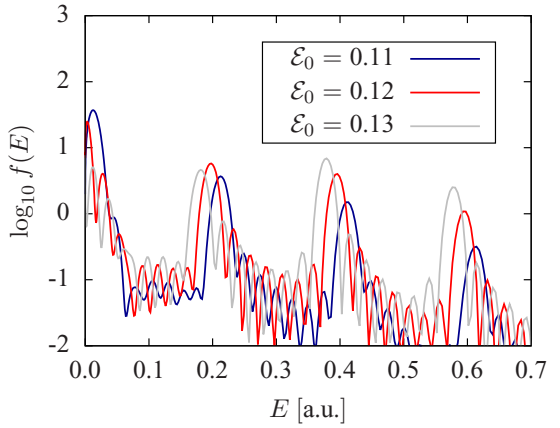

FIG. 2. (Color online) Laser-driven ($\omega = 0.2$, $t = 8T$) energy distribution function for different laser strengths.

B. Wigner representation of laser-induced ionization

Equation (9) has been used to determine the Wigner function from the free states (12). In agreement with the definition of the spectral density, left and right moving electrons are equally considered. In the Wigner approach, an energy-position distribution function can be defined by

$$W(E,q) = |p|^{-1}\{W(p,q) + W(-p,q)\}. \tag{14}$$

Position-energy correlations are finally discussed by plotting $W(E,q)$ versus q and $E = p^2/2$. Figure 3 shows the dependence of the Wigner function on the electric field $\mathcal{E}_0$ for a laser with frequency $\omega = 0.2$ after the interaction time of eight laser periods. Positive values of the distribution function are red (light-gray) and negative ones are blue (dark-gray). One can recognize the emergence of horizontal red (light-gray) beams, e.g., observable for an energy of $E \approx 0.4$ in Fig. 3.

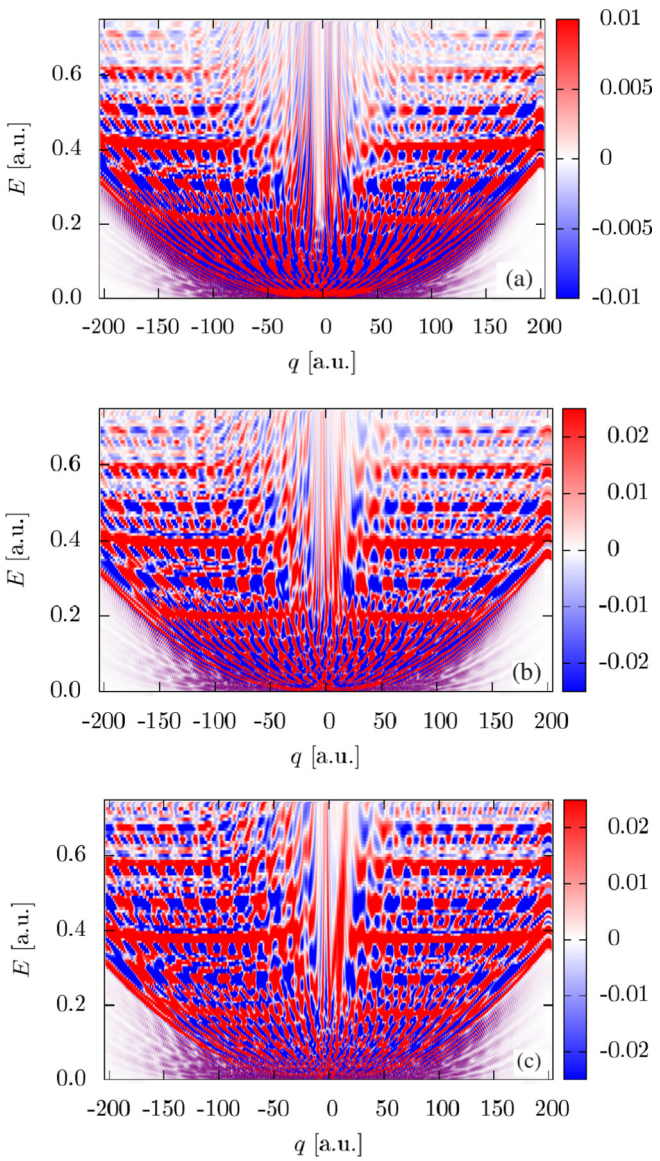

FIG. 3. (Color online) Wigner function for laser field strengths (a) $\mathcal{E}_0 = 0.11$, (b) $\mathcal{E}_0 = 0.12$, and (c) $\mathcal{E}_0 = 0.13$ (frequency $\omega = 0.2$) after an interaction time of eight laser periods.

These beams can be understood as plane-wave states for the ATI peaks of the spectrum (Fig. 2). This correspondence can be explained by the relation

$$\int_{-\infty}^{\infty} dq\, W(p,q) = |\hat{\phi}_{\text{free}}(p)|^2. \tag{15}$$

Consequently, the integration of the Wigner function $W(E,q)$ along the q axis determines the spectral density function $f(E)$. Horizontal red (light-gray) beams contribute significantly to the value of the integral and thereby lead to the observed energy peaks. The emergence of ATI peaks also allows for the identification of channel closing in the Wigner function, expressed by the disappearance of the low-energy peak in Fig. 3(c).

Apart from the plane-wave states and the channel closing, the formation of another interference pattern is visible in the quasiprobability function. Plane-wave states with different momenta p (corresponding to different energies E) interfere, yielding an alternating series of blue and red (dark- and light-gray) areas in the subspace between two beams. The Wigner representation of plane waves has been discussed previously in our group [22]. The interference pattern describes a quantum-mechanical wave along the q direction that propagates with the mean momentum $\bar{p}$ of the interfering states. The associated wavelength is determined by the difference momentum Δp of the interfering states which is accompanied by an energy shift. This shift can be expressed in terms of an integral multiple s of the photon energy as described in the Introduction,

$$\Delta E = \bar{p}\,\Delta p \equiv s\omega. \tag{16}$$

Restricting attention to the most dominant interference channel $s = 1$, the wavelength can be written as

$$\lambda_q = \frac{2\pi}{\Delta p} = \bar{p}T, \tag{17}$$

and is therefore equal to the distance that a particle with momentum $\bar{p}$ moves during one laser period. The wavelength (17) of the quantum-mechanical interference pattern clearly corresponds to the classical bunch length of density modulations by the laser field. Finally, numerical evaluations yield $\lambda_q \approx 31$ for energies $E = 0.4$ and $E = 0.6$, which is in agreement with the data shown in Fig. 4. Here, the interference structure has been transformed to the q space by integrating the Wigner function in a small vicinity around $\bar{E} = \bar{p}^2/2$,

$$g(q) = \int_{\bar{E}-\delta E}^{\bar{E}+\delta E} dE\, W(E,q), \tag{18}$$

which nicely visualizes the wavelength λ_q. One can also recognize the maximum extension up to the travel distance $d_{\max} = 8\bar{p}\,T \approx 249$ within the interaction time of eight periods.

As a further remark, we consider the influence of interference channels with $s \neq 1$. In this case, it is possible that the energy $\bar{E}$ coincides with one of the ATI peaks. The corresponding interference pattern leads to a modulation of the height of the ATI peak. We have seen such modulations previously in the discussion of the spectral density function.

Finally, we show the Wigner function in the phase-space area in the vicinity of the atom in Fig. 5. The parameters are

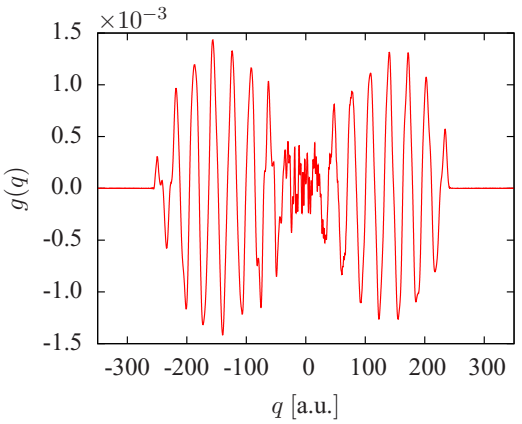

FIG. 4. (Color online) Results of the integral (18) with parameters $\bar{E} \approx 0.5$ and $\delta E = 0.02\,\bar{E}$. One can clearly recognize the wavelength $\lambda_q \approx 31$.

the same as in the large-scale representation of Fig. 3. We also indicate in the figure the separatrix (20) between classically free and bound states. Since the bound state has been removed from the wave function by the projection method, the Wigner function gives a phase-space representation of the free ATI electrons after ionization. Before channel closing [Fig. 5(a)], one can recognize that the probability of electrons near the top of the separatrix is quite low, corresponding to a white area there [note the magnified color (gray) scale used in (a)]. During channel closing, low-energy electrons are produced that populate a band with positive probability along the separatrix line [Figs. 5(b) and 5(c)]. This increase of low-energy electrons is also consistent with an increase in the bound-state population, considered in the following Sec. IV.

IV. BOUND-STATE POPULATION IN PHASE SPACE

We now present a method that quantifies the bound-state population of a system by using the Wigner function. The method is based on a quasiclassical approximation of the dynamics at the ionization threshold in the phase space.

A. Wigner-function method

We first consider a classical particle within the Rosen-Morse potential $V(q)$, given in (6). Its dynamics can be obtained by studying its total energy in the laboratory system,

$$E = \tfrac{1}{2}p^2 + V(q). \tag{19}$$

From a classical point of view, positive energies ($E > 0$) lead to free orbits and negative energies ($E < 0$) to bound orbits. Consequently, $E = 0$ defines the separatrix line,

$$p = \pm\sqrt{2\,|V(q)|}, \tag{20}$$

that separates the bound and unbound regions from each other. A quasiclassical estimate of the bound-state population is now defined by integrating the Wigner quasiprobability density over the phase-space region enclosed by the classical

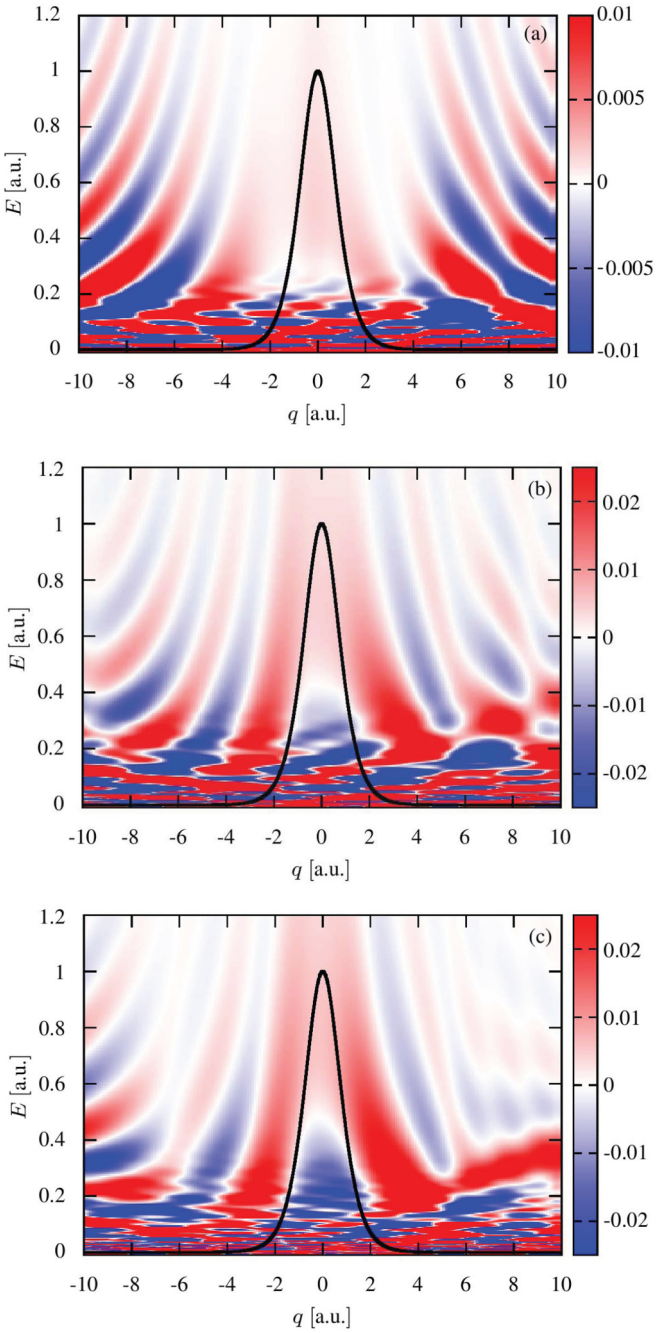

FIG. 5. (Color online) Wigner function near the classical separatrix (solid line) between free and bound states for laser field strengths (a) $\mathcal{E}_0 = 0.11$, (b) $\mathcal{E}_0 = 0.12$, and (c) $\mathcal{E}_0 = 0.13$ (frequency $\omega = 0.2$) after an interaction time of eight laser periods.

separatrix,

$$\Gamma_{\text{bound}} = \int_{-\infty}^{\infty} dq \int_{-p(q)}^{p(q)} \frac{dp}{2\pi}\, W(p,q). \tag{21}$$

For classical systems, (21) corresponds to the exact population of bound states which follows from Liouville's theorem and the fact that classical trajectories do not intersect each other. However, the method is extended to determine also the bound-state population of laser-driven quantum systems. In these systems, Γ_{bound} is evaluated only at the zeros of

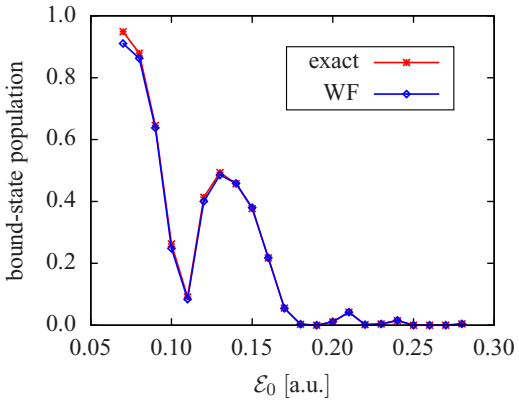

FIG. 6. (Color online) Dependence of the bound-state population [atom modeled by Eq. (6)] on the field strength $\mathcal{E}_0$ for a sine wave with frequency $\omega = 0.2$ after a fixed interaction time of $8T$. Data points have been recorded by using the exact projection (cross symbols) and the Wigner-function method (diamond symbols).

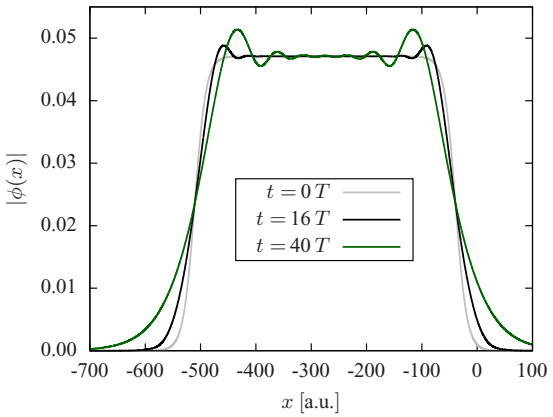

FIG. 7. (Color online) Evolution of the electron wave function under free propagation in the absence of a laser field and of an atomic potential. The initial wave packet ($t = 0$) is compared to the wave packets after the propagation times $t = 16T$ and $t = 40T$ measured in units of the laser period T. For visual convenience, the propagated wave functions are shifted backwards by the propagation distance $\Delta x = k_0 t$. One can recognize the evolution of two humps at the edges of the distribution. Parameters are $k_0 = 0.25$, $T = 2\pi/\omega \approx 31.4$, $x_r = -5k_0T$, $x_l = x_r - 60k_0T$, and $\Delta_r = -\Delta_l = (0.6/\ln 10)\,|x_r|$.

the electric field such that the classical energy is given by (19). Additionally, note that the Wigner function has to be calculated from the full time-propagated states in the laboratory system, where canonical and physical momenta coincide. One obtains the corresponding wave functions by reversing the KH transformations (3) and (4).

To verify the applicability of the presented method, test calculations have been performed. Equation (6) is used again as a model potential, and Fig. 6 finally shows the results for the bound-state population, determined by using the Wigner function (diamond symbols) and the exact quantum-mechanical approach [cross symbols, representing the square of the absolute value of ρ; see Eq. (12)]. One can immediately recognize that the Wigner-function (WF) approach determines the bound-state population with high accuracy.

B. Application to laser-driven scattering

We now consider the laser-driven ($\mathcal{E}_0 = 0.2$, $\omega = 0.2$) scattering by the model potential. Therefore the electron is prepared in a free initial state that moves with a drift momentum k_0 towards the potential. The initial state is represented by a plane wave that is modified with a spatial envelope function, $\phi(x) = f(x)e^{ik_0x}$. In the simulations, the initial drift momentum has been chosen small in comparison to the typical quiver momentum ($k_0 = 0.25\,\dot{\xi}_0$) such that it should be possible to observe significant recombination [7,8]. The spatial envelope, shown in Fig. 7, is made up of two Fermi functions

$$f(x) = C f_r(x) f_l(x), \quad f_{r,l}(x) = \frac{1}{\exp\left(\frac{x - x_{r,l}}{\Delta_{r,l}}\right) + 1}, \qquad (22)$$

where C is a normalization constant and the parameters $x_{r,l}$, $\Delta_r > 0$, $\Delta_l < 0$ model a smooth incidence of the electron, followed by a plateau. The long plateau symbolizes a constant probability current and can be used to study the steady state of recombination-ionization dynamics. However, one has to keep in mind, that the free propagation of the wave packet leads to some modifications of its shape. This can be seen from Fig. 7, where the initial wave function at $t = 0$ is compared to the shapes of the freely propagated wave functions at the times $t = 16T$ and $t = 40T$. The wave functions develop an interference pattern with two large humps at the edges of the distribution. This same structure will subsequently be observed in the time dependence of the laser-induced bound-state population.

In the absence of the laser field recombination is negligible. This follows from the fact that the potential is reflectionless under stationary conditions and the stationary state is achieved by the smooth turn-on and turn-off of the incident beam. This has also been verified numerically by the projection method. With laser field a significant fraction of the incident beam recombines. The dynamics of the bound-state population is shown in the upper panel of Fig. 8, again obtained by using the exact (black curve) and the WF method [red (light-gray) curve]. From a qualitative point of view, both approaches predict the same behavior. In the beginning, the bound-state population increases due to the smooth incidence of the electron beam. The subsequent stationary bound-state population is of particular importance. Recombination and ionization balance each other as long as the constant part of the probability current interacts with the ion. This leads effectively to a kind of steady state in the system. The steady state exists until the incoming probability current decreases ($t \approx 55T$), which finally results in an exponential depopulation of the bound state. Quantitatively, one can see that the WF approach slightly overpredicts the bound-state population for the discussed laser parameters.

One can observe transient overshoots of the bound-state population after approximately 12 and 55 laser periods. These overshoots can be attributed to the humps at the edges of the electron wave packet in Fig. 7. Note that the two humps in the bound-state population are different, occurring at the same position but at different times. The lower front hump arrives earlier and the higher rear hump later at the position of the ion.

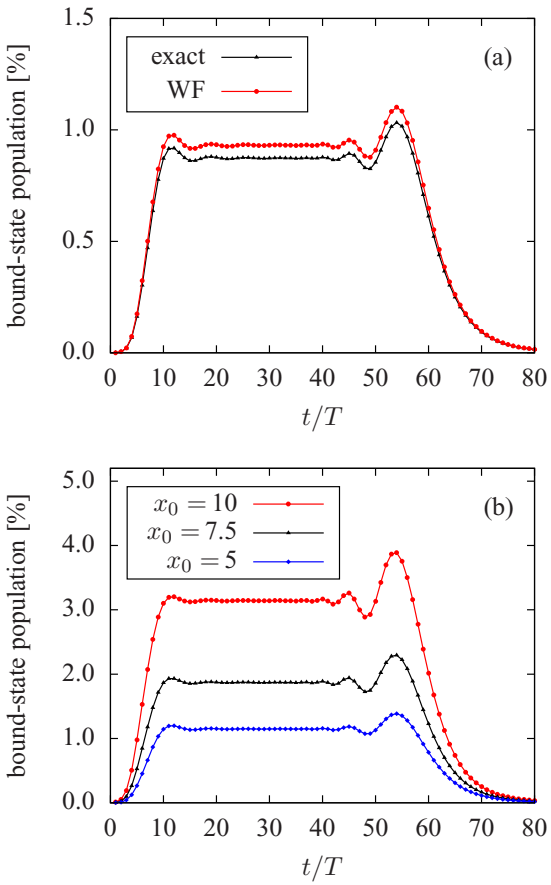

FIG. 8. (Color online) Time dependence of the bound-state population, recorded for the laser-driven ($\mathcal{E}_0 = 0.2$, $\omega = 0.2$) scattering of slow electrons ($k_0 = 0.25\,\dot{\xi}_0$) by the model potential (6). Data points are calculated with (a) the exact projection method, the WF approach and (b) the spatial-filter approximation.

One can convince that the humps in both figures are actually coincident. The propagation times $t/T = 16{,}40$ correspond to propagation distances $\Delta x = 125{,}314$, respectively. At the time $t = 16T$ the first hump has just passed; at the time $t = 40T$ the second hump is just approaching the ion.

To be able to assess the improvements gained by the presented approach, a comparative analysis has been performed with another well-established method. Spatial filters, which assume that only electrons in a small vicinity x_0 around the atomic center are bound, approximate the bound-state population as

$$\Gamma'_{\text{bound}} = \int_{-x_0}^{x_0} dx\, |\phi(x)|^2. \tag{23}$$

Values of $x_0 = 5$, 7.5, and 10 have been used in the simulations. The results are given in the lower panel of Fig. 8, all showing the previously described behavior of the bound-state population. However, one can recognize that the bound-state population deviates already at the edges and strongly depends on the selected parameter x_0. Considering in particular $x_0 = 7.5$ and 10, the spatial filter predicts a much too high binding fraction. Only for $x_0 = 5$, Γ'_{bound} accidentally offers similar results as those found with the exact and the WF method. These differences result from the instantaneous evaluation of (23). Free parts of the wave function, which are located in the center of the grid, do not have enough time to leave this region and are thus counted erroneously as bound part. In contrast, the phase-space method allows for an instantaneous approximation concerning calculations of the bound-state population and is not as arbitrary as the spatial method, which depends sensitively on the boundaries of the integration region.

C. Extension to spherically symmetric potentials in three dimensions

We now extend the WF approach for the bound-state population to the physically interesting case of three-dimensional (3D) potentials. The Wigner function for a 3D wave function is defined on a six-dimensional phase space and its calculation would be extremely expensive. However, for spherically symmetric potentials, one can reduce the problem to a set of 1D radial wave equations and their corresponding Wigner functions. In this case the WF method becomes again advantageous in comparison with the projection method. We therefore consider a spherically symmetric potential and choose the hydrogen atom as an example. In the following it is demonstrated that the WF method gives accurate results for various bound states of hydrogen.

Due to the study of spherically symmetric potentials, we expand the wave function in terms of spherical harmonics $Y_{lm}(\theta,\phi)$,

$$\psi(r,\theta,\phi,t) = \sum_{l,m} \frac{1}{r}\, \chi_{lm}(r,t)\, Y_{lm}(\theta,\phi), \tag{24}$$

where $\chi_{lm}(r,t)$ is the radial wave function that contains all information about occupied or unoccupied states of the system. In the absence of a laser field ($\mathcal{E}_0 = 0$), one obtains from (24) for each set (l,m) of quantum numbers a 1D Schrödinger equation for the radial part,

$$\begin{aligned} i\,\partial_t\, \chi_{lm}(r,t) &= \left\{ -\frac{1}{2}\partial_r^2 + V^l_{\text{eff}}(r) \right\} \chi_{lm}(r,t), \\ V^l_{\text{eff}}(r) &= V(r) + \frac{l(l+1)}{2r^2}. \end{aligned} \tag{25}$$

Using the exact method, the bound-state population for a given wave function $\psi(r,\theta,\phi,t)$ is defined by the sum over all bound-state probabilities of the various quantum sets (n,l,m). The occupation of one bound state is now determined by the projection of the corresponding eigenfunction $\psi_{\text{nlm}}(r,\theta,\phi) = Y_{lm}(\theta,\phi)\, u_{nl}(r)/r$ on the full wave function,

$$\Gamma_{\text{nlm}} = \left| \int d^3r\, \psi^*_{\text{nlm}}\, \psi \right|^2 = \left| \int_0^\infty dr\, u_{nl}(r)\, \chi_{lm}(r) \right|^2, \tag{26}$$

where we have used the orthogonality of the spherical harmonics and the real character of the radial eigenfunctions $u_{nl}(r)$. The total bound-state population is given by the sum

$$\Gamma_{\text{bound}} = \sum_{n,l,m} \Gamma_{\text{nlm}} = \sum_{l,m} \left(\sum_n \Gamma_{\text{nlm}} \right) = \sum_{l,m} \Gamma_{lm}, \tag{27}$$

where we have defined the orbital population Γ_{lm}. Considering (25)–(27), one can clearly recognize the equivalence to pure

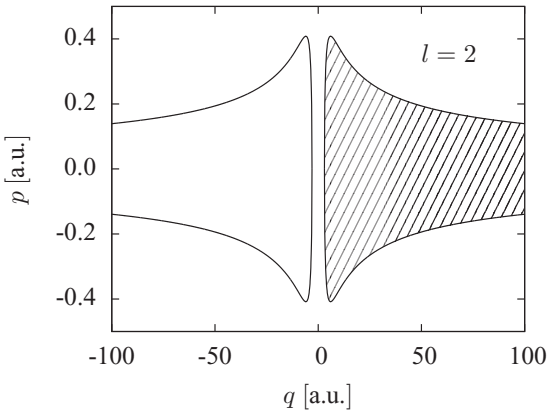

FIG. 9. Section of the bound-state region (hydrogen atom) for angular-momentum $l = 2$. The shaded part represents the domain of integration for spherically symmetric potentials.

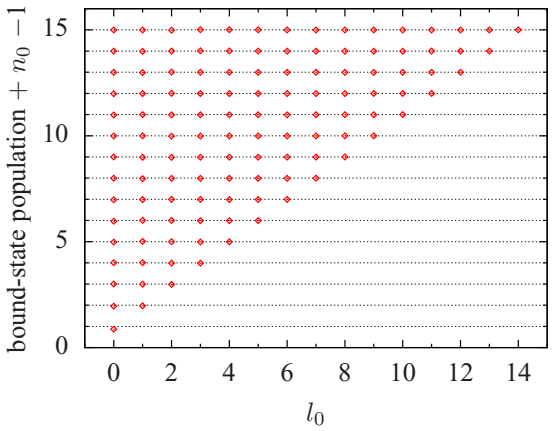

FIG. 10. (Color online) Results for the bound-state population that are obtained for different stationary states of the hydrogen atom with the WF method. For visual convenience the results for different radial quantum numbers n_0 are shifted by $n_0 - 1$. The exact values are therefore given by $1 + n_0 - 1 = n_0$ in this representation.

1D systems. Consequently, we can approximate Γ_{lm} by using the WF approach for the radial function $\chi_{lm}(r)$ in the potential $V^l_{\text{eff}}(r)$. However, the domain of definition for the Wigner function requires some extension because of the restriction $r \geqslant 0$ for the radial wave function. For this purpose, we extend the radial wave function to a negative r axis by using the symmetry properties of the space-inverted wave function $\psi(r,\pi - \theta,\phi + \pi,t)$,

$$\tilde{\chi}_{lm}(r) = \begin{cases} \chi_{lm}(r), & r \geqslant 0, \\ (-1)^l\, \chi_{lm}(|r|), & r < 0. \end{cases} \tag{28}$$

Using these states, the Wigner function and the phase-space integral (21) can be evaluated for the effective potential $V^l_{\text{eff}}(r)$. To calculate the bound-state population correctly, (21) has to be multiplied by an additional factor one-half which accounts for the normalization of $\tilde{\chi}_{lm}$. Alternatively, based on the symmetry properties (28), the physical bound-state population is obtained if one restricts the domain of integration in (21) to the positive half space $q \geqslant 0$ (see Fig. 9), thereby reducing the numerical effort. Note that the computational effort is also reduced for linearly polarized fields since the magnetic quantum number m is conserved.

Test calculations have been performed by assuming that the system is in a stationary bound state (n_0,l_0,m_0) of the hydrogen atom. In the following $m_0 = 0$ is chosen in all simulations. In this case, the radial wave function is equal to $\chi_{lm}(r) = r R_{n_0,l_0}(r)\delta_{l,l_0}\delta_{m,m_0}$. Figure 10 finally shows the results for different quantum numbers (n_0,l_0). One can see that the WF approach yields populations in a small vicinity around 1. Significant deviations can only be observed for the ground state of the hydrogen atom, where the WF method deviates about 15% from the exact result. Therefore, for future applications of this method it is advisable to calculate the ground-state population exactly by the projection method and to remove subsequently this projection from the full wave function. The numerical effort does not increase significantly. We have also verified the procedure for a few superpositions of bound states and found similar accuracy as for the individual states in the superposition. It is further noted that the radius of the Bohr orbit for quantum number n is $r = n^2$ and therefore equal to $r = 225$ for the maximum quantum number $n = 15$. Evidently, a comparable accuracy of the bound-state population could not be achieved with spatial filter methods assuming atomic radii of the order of 1–10.

V. CONCLUSION

In the present work, the Wigner representation of ionization has been discussed by solving the TDSE for a 1D model atom. Energy spectra, which can be measured outside the laser field, have been evaluated as a function of the electric field amplitude, nicely showing the Stark shift of the continuum states. The Wigner function of the freed electron displays the emergence of ATI peaks by forming plane-wave-like states. The interference of plane waves leads to typical fringes that could be observed in the corresponding Wigner representation. The phase-space visualization of ATI peaks has enabled the identification of channel closing in the model system.

In addition, a method has been introduced that can be used to determine the bound-state population of a quantum system with the assistance of the quasiprobability density. This approach is not as arbitrary as the well-known spatial approximation and enables the possibility of calculating the binding fraction instantaneously at the zeros of the laser field. One does not need to wait for an asymptotic state where free and bound parts of the wave function become separated. Using the present method, it has been also possible to resolve a steady state in the system while subjecting the ion to a stationary probability current in a laser field.

In the final part of this work, we have indicated the extension of the WF method to calculate the bound-state population of more realistic 3D atoms with spherical symmetry.

ACKNOWLEDGMENTS

Allocation of CPU time and assistance by the computer facilities from the IT Center of the RWTH Aachen University are acknowledged.

[1] D. Bauer, T. Brabec, H. Fehske, S. Lochbrunner, K. Meiwes-Broer, and R. Redmer, New J. Phys. **15**, 065015 (2013).
[2] P. Agostini, F. Fabre, G. Mainfray, G. Petite, and N. K. Rahman, Phys. Rev. Lett. **42**, 1127 (1979).
[3] P. A. Franken, A. E. Hill, C. W. Peters, and G. Weinreich, Phys. Rev. Lett. **7**, 118 (1961).
[4] L. Schlessinger and J. Wright, Phys. Rev. A **20**, 1934 (1979).
[5] T. Bornath, M. Schlanges, P. Hilse, and D. Kremp, Phys. Rev. E **64**, 026414 (2001).
[6] H.-J. Kull and L. Plagne, Phys. Plasmas **8**, 5244 (2001).
[7] G. Rascol, H. Bachau, V. Tikhonchuk, H.-J. Kull, and T. Ristow, Phys. Plasmas **13**, 103108 (2006).
[8] G. M. Fraiman, V. A. Mironov, and A. A. Balakin, Phys. Rev. Lett. **82**, 319 (1999).
[9] D. A. Serebryakov, A. A. Balakin, and G. M. Fraiman, Plasma Phys. Rep. **40**, 705 (2014).
[10] M. Lewenstein, P. Balcou, M. Y. Ivanov, A. LHuillier, and P. B. Corkum, Phys. Rev. A **49**, 2117 (1994).
[11] P. Salières, B. Carré, L. Le Déroff, F. Grasbon, G. Paulus, H. Walther, R. Kopold, W. Becker, D. Milošević, A. Sanpera *et al.*, Science **292**, 902 (2001).
[12] A. Goldberg, H. M. Schey, and J. L. Schwartz, Am. J. Phys. **35**, 177 (1967).
[13] K. C. Kulander, Phys. Rev. A **35**, 445 (1987).
[14] D. Bauer and P. Koval, Comput. Phys. Commun. **174**, 396 (2006).
[15] E. Wigner, Phys. Rev. **40**, 749 (1932).
[16] N. Rosen and P. M. Morse, Phys. Rev. **42**, 210 (1932).
[17] J. B. Watson, C. H. Keitel, P. L. Knight, and K. Burnett, Phys. Rev. A **54**, 729 (1996).
[18] A. Czirjak, R. Kopold, W. Becker, M. Kleber, and W. Schleich, Opt. Commun. **179**, 29 (2000).
[19] A. Czirják, S. Majorosi, J. Kovács, and M. G. Benedict, Phys. Scr. T **153**, 014013 (2013).
[20] C. Zagoya, J. Wu, M. Ronto, D. Shalashilin, and C. F. de Morisson Faria, New J. Phys. **16**, 103040 (2014).
[21] M. Lein, V. Engel, and E. Gross, Opt. Express **8**, 411 (2001).
[22] H. Kull, New J. Phys. **14**, 055013 (2012).
[23] J. E. Moyal, in *Mathematical Proceedings of the Cambridge Philosophical Society* (Cambridge University Press, Cambridge, UK, 1949), Vol. 45, pp. 99–124.
[24] D. Bauer, Phys. Rev. A **56**, 3028 (1997).
[25] J. L. Sanz and H.-J. Kull, Phys. Rev. A **60**, 3896 (1999).
[26] M. Heinen and H.-J. Kull, Phys. Rev. E **79**, 056709 (2009).
[27] L. Tao and A. Scrinzi, New J. Phys. **14**, 013021 (2012).
[28] P. Agostini and L. F. DiMauro, Phys. Rev. A **47**, R4573 (1993).
[29] K. J. Schafer and K. C. Kulander, Phys. Rev. A **42**, 5794 (1990).
[30] K. Schafer, Comput. Phys. Commun. **63**, 427 (1991).
[31] W. C. Henneberger, Phys. Rev. Lett. **21**, 838 (1968).
[32] H. A. Kramers, *Collected Scientific Papers* (North-Holland, Amsterdam, 1956).
[33] R. K. Dodd, J. C. Eilbeck, J. D. Gibbon, and H. C. Morris, *Solitons and Nonlinear Wave Equations* (Academic Press, Inc., London-New York, 1982), pp. 71–73.
[34] J. Fleck, Jr., J. Morris, and M. Feit, Appl. Phys. **10**, 129 (1976).
[35] V. Ayvazyan *et al.*, Phys. Rev. Lett. **88**, 104802 (2002).
[36] S. Chakrabarti, H. Muench, and T. Halfmann, Phys. Rev. A **82**, 063817 (2010).